



# Application of Low-Rank Tensor Completion Combined with Prior Knowledge in Visual Data

Junzhe Zhao<sup>1</sup>, Huimin Wang<sup>\*2</sup>

School of Mathematics Information, Shaoxing University, 312000 Shaoxing, China

\* Correspondence: Huimin Wang (glanme@usx.edu.cn)

**Received:** 11-10-2024**Revised:** 12-19-2024**Accepted:** 12-25-2024**Citation:** J. Z. Zhao and H. M. Wang, "Application of low-rank tensor completion combined with prior knowledge in visual data," *Acadlore Trans. Mach. Learn.*, vol. 3, no. 4, pp. 237–251, 2024. <https://doi.org/10.56578/ataiml030405>.

© 2024 by the author(s). Published by Acadlore Publishing Services Limited, Hong Kong. This article is available for free download and can be reused and cited, provided that the original published version is credited, under the CC BY 4.0 license.

**Abstract:** In recent years, representing computer vision data in tensor form has become an important method of data representation. However, due to the limitations of signal acquisition devices, the actual data obtained may be damaged, such as image loss, noise interference, or a combination of both. Using Low-Rank Tensor Completion (LRTC) techniques to recover missing or corrupted tensor data has become a hot research topic. In this paper, we adopt a tensor coupled total variation (t-CTV) norm based on t-SVD as the minimization criterion to capture the combined effects of low-rank and local piecewise smooth priors, thus eliminating the need for balance parameters in the process. At the same time, we utilize the Non-Local Means (NLM) denoiser to smooth the image and reduce noise by leveraging the nonlocal self-similarity of the image. Furthermore, an Alternating Direction Method of Multipliers (ADMM) algorithm is designed for the proposed optimization model, NLM-TCTV. Extensive numerical experiments on real tensor data (including color, medical, and satellite remote sensing images) show that the proposed method has good robustness, performs well in noisy images, and surpasses many existing methods in both quality and visual effects.

**Keywords:** Tensor completion; t-SVD decomposition; Nuclear norm minimization; Image processing

## 1 Introduction

Humans are more inclined to accept high-quality, high-resolution images due to their rich visual senses. Clear images are not only pleasing to the eye but also allow for the extraction of more precise information and features. However, in some special environments, the quality of images cannot be guaranteed. Noise often appears in images, which originally referred to a type of sound that hinders auditory perception and thinking. Image noise is a factor that interferes with the information in an image, often causing the image to blur. For example, image blur can be caused by object motion, adverse weather conditions, poor lighting, camera issues leading to distortion, or image damage. To address these issues, we typically model computer images as matrices or tensors, depending on the dimensions and features of the images. As the amount of information contained in computer images increases, the dimensionality of computer vision data continues to rise. We usually model high-dimensional data as tensors, which can capture and represent the intrinsic structure of high-dimensional data, thereby improving accuracy and efficiency in various data analysis tasks. The processing of multidimensional arrays is currently a hot research topic. Tensor processing has shown powerful capabilities in signal processing [1], data mining [2], machine learning [3, 4], and computer vision [5–7].

The handling of tensor issues can be traced back to one-dimensional signal processing. In 2004, Donoho proposed the theory of compressed sensing [8], which uses the sparsity of signals to recover the desired signals with fewer samples. In 2005, Candes and Tao proposed the Restricted Isometry Property (RIP) [9]. RIP describes the relationship between the properties of the measurement matrix and the performance of sparse signal recovery and is an important concept in the field of compressed sensing. Since the data of digital tensors modeled from images are often large, directly processing them can be very costly. In practice, computer images usually have non-local self-similarity, which promotes the low-rank or approximate low-rank nature of computer images. In addressing the problem of low-rank tensor image enhancement, modeling it as a Low Rank Tensor Completion (LRTC) problem is a common

approach. The tensor completion model can be mathematically formulated as follows:

$$\min_{\mathcal{X}} \text{rank}(\mathcal{X}) \quad \text{s.t.} \quad \mathcal{P}_{\Omega}(\mathcal{X}) = \mathcal{P}_{\Omega}(\mathcal{Y}) \quad (1)$$

where,  $\mathcal{X}$  is the tensor to be solved,  $\mathcal{Y}$  is the observed tensor,  $\Omega$  is the set of indices of the observed elements, and  $\text{rank}(\cdot)$  is the tensor rank function.

When studying the problem of matrix completion, the handling of rank is a key aspect. Similarly, in the context of low-rank tensor completion, dealing with tensor rank is crucial. The CP rank and Tucker rank are two commonly used tensor ranks in tensor processing. In the tensor recovery based on CP rank minimization [10], CP decomposition decomposes a tensor into a set of rank-1 tensors. Accurately computing the CP rank of tensor data is typically NP-hard. Additionally, accurately finding the convex relaxation of the CP rank is challenging [11], making low CP rank tensor recovery difficult. Tensor recovery based on (Sum of Nuclear Norms Tensor Completion, SNN) minimization derived from Tucker rank [12, 13], Tucker decomposition can perform dimensionality reduction for different patterns, making it very flexible when dealing with complex data structures. However, the computational complexity of this decomposition is relatively high, and choosing the appropriate core tensor size and factor matrix ranks is challenging. Overall, exploring tensor ranks and their effective computation forms in certain decomposition schemes remains an open topic.

In recent years, with Kilmer proposing the t-SVD framework for tensors [14], new methods for tensor completion have emerged. t-SVD decomposes a tensor into the t-product of two orthogonal tensors and a f-diagonal tensor (also known as the singular value tensor), resulting in a new tensor rank, the tubal rank. This rank is defined as the number of non-zero singular tubes in the singular value tensor. Compared to traditional tensor decomposition strategies, the t-SVD scheme has been proven to perform excellently in capturing the spatial correlations and global structure information commonly present in real-world tensor data [15, 16]. Tensor t-SVD decomposition offers a good low-rank approximation, retaining the multi-dimensional structure information of the tensor, ensuring that the decomposed tensor still possesses the high-order characteristics of the original data. This helps preserve the complex relationships and dependencies in the data, some regularization terms based on tubular rank are suitable for tasks such as tensor completion and compression [17, 18]. Consequently, recent research has focused on tubal rank minimization, and tubal rank minimization has shown promising results in practical applications like image restoration.

However, common computer images to be completed may contain noise. Unlike pure denoising tasks, where the pixels of the missing blocks overlap with noise, such noisy completion tasks are more complex. Some common completion methods have some noise suppression effects, but the expected results are not achieved after completion. To address this problem, this paper proposes an efficient low t-SVD rank TC model. Utilizing the non-local self-similarity property of images, the Non-Local Means (NLM) denoiser [19] is used to denoise the observed pixels of the original image, followed by the completion of the image aggregated from the denoised image blocks. This achieves both denoising and completion of the image.

The main contributions can be summarized as follows:

- In the t-SVD framework, this paper proposes a tensor completion model based on t-CTV regularization combined with the NLM denoising method, designed to handle data with overlapping noise and missing entries, referred to as NLM-TCTV. We apply NLM to the non-missing data of the tensor, utilizing the self-similarity prior of the image, while simultaneously performing denoising and smoothing, thereby improving the performance of the t-CTV method. For our tensor completion model, based on the general definition of the tensor t-product for invertible linear transformations, the relevant algebraic structures of our tensor completion model are as follows.

- For images with overlapping noise and missing information, directly using denoising methods often results in the denoising of missing pixels as well, which is detrimental to image quality improvement. The proposed new method has yielded encouraging outcomes in completing tasks for color images, medical images, and satellite images. Compared to the classical TC method, our method increases the average PSNR value by approximately 2-4 dB. Experiments conducted under different missing rates and noise levels show good robustness of the method, with the images completed by NLM-TCTV displaying more details and features than those completed by other methods. Additionally, the completion algorithm demonstrates strong recovery performance even at high missing rates (90%).

The arrangement of this paper is as follows: The second section introduces related work on tensor completion. The third section describes the model construction in detail, including the t-SVD decomposition and the preliminary knowledge and theoretical support of the model. The fourth section proposes the noisy tensor denoising completion model NLM-TCTV and solves it using the ADMM algorithm. The fifth section evaluates the effectiveness of the proposed algorithm through extensive experiments. Finally, the sixth section summarizes our work and suggests future research directions.

## 2 Related Work

For Tucker decomposition, Liu et al. [20] first developed the nuclear norm of the tensor unfolding matrix (Sum of Nuclear Norms Tensor Completion, SNN) as a convex envelope of the tensor Tucker rank, and established a low-rank

tensor completion model (LRTC) based on SNN. They proposed three optimization algorithms (SiLRTC, FaLRTC, and HaLRTC). These three image completion algorithms are characterized by fast convergence, easy implementation, and high efficiency, and are widely used in image processing. Goldfarb and Qin [21] applied this idea to the principal component analysis (PCA) problem, proposing a tensor robust principal component analysis (TRPCA) model, which improved the effect of tensor recovery. Bengua et al. [22] improved the SiLRTC algorithm in SNN and proposed new optimization formulas for tensor completion, as well as two new algorithms to solve them. In recent years, Zhang [23] used a series of non-convex functions on the singular values of the squared matrix of tensors to approximate the tensor Tucker rank, and then proposed a non-convex model called the Nonconvex Relaxation Approach to Low-Rank Tensor Completion (NRATC) for LRTC.

For t-SVD decomposition directly minimizing the tubular rank is NP hard [11], necessitating the development of a norm as a convex surrogate for the tubal rank. Semerci et al. [24] developed a heuristic tensor nuclear norm (TNN) as its convex surrogate in the Fourier domain. Zhang and Aeron [25] applied TNN to tensor completion, investigating the tubal rank TC problem. Lu et al. [26] defined the average rank of a tensor, and derived that when a tensor has a low tubal rank, its average rank will correspondingly be low. They also proposed an innovative tensor nuclear norm minimization model, which was proven to be the convex envelope of the tensor spectral norm unit ball corresponding to the average rank of tensors in the Fourier domain. Lu et al. [27] proposed a more general definition of tensor rank and applied its corresponding convex relaxation to third-order tensor completion, demonstrating better performance in many completion tasks compared to other types of tensor nuclear norms. In recent studies on completion problems, Pan et al. [28] utilized a weighted nuclear norm with multiple regularization terms, proposing a low-rank minimization model induced by sparse and weighted nuclear norms based on DCT, achieving good results at low sampling rates. Wang et al. [29] proposed the TCTV model using low-rank and smoothness priors and applied the model to the two classical tasks of TC and TRPCA, achieving good results.

Other tensor decomposition methods, such as tensor-train (TT) decomposition-based completion, are suitable for high-dimensional tensors, addressing the completion problem for tensor data with high-dimensional structures. Xu et al. [30] approached TT decomposition from a fully Bayesian perspective, including automatic TT rank determination and noise power estimation, thereby recovering the underlying TT structure. For tensor-ring (TR) decomposition, Wu et al. [31] considered low-rank and sparsity priors of gradient factors to enhance the performance and robustness of TR decomposition-based models. In summary, tensor decomposition-based tensor completion methods are continuously evolving, and more decomposition methods and regularization terms will likely be applied to completion tasks in the future.

### 3 Preliminary Knowledge

Firstly, let  $\mathcal{M}$  be a color image corrupted by noise and missing pixels. Consider the three-dimensional tensor  $\mathcal{M} \in \mathbb{R}^{I \times J \times K}$  as the three-dimensional image we need to denoise and complete. During the NLM process, considering the self-similarity of the image, we need to search for similar patches in the image and categorize them into  $N$  classes based on similarity. This three-dimensional tensor  $\mathcal{M}$  is unfolded along its third mode into  $m$  subblocks, with each segmented sub-tensor block denoted as  $\mathcal{M}_i \in \mathbb{R}^{d_I \times d_J \times K}$ , ( $i = 1, 2, 3, \dots, m$ ), where  $d_I \times d_J$  represents the size of a single sub-block. During the segmentation of the data blocks, the sub-blocks overlap. The total data volume of these sub-blocks is  $m \times d_I \times d_J \times K$ , which is greater than the original data volume  $I \times J \times K$ . The overlap data volume  $L$  determines  $m$  and is given by

$$m = \left\lceil \frac{I \times J \times K + L}{d_I \times d_J \times K} \right\rceil$$

**Definition 1.** (T-product [14]) For two third-order tensors  $\mathcal{X} \in \mathbb{R}^{n_1 \times n_2 \times n_3}$  and  $\mathcal{Y} \in \mathbb{R}^{n_2 \times n_4 \times n_3}$ , the  $t$ -product  $\mathcal{Z} \in \mathbb{R}^{n_1 \times n_4 \times n_3}$  is defined as:

$$\mathcal{Z} = \mathcal{X} * \mathcal{Y} = \text{fold}(\text{bcirc}(\mathcal{X}) \cdot \text{unfold}(\mathcal{Y}))$$

where, the block circulant matrix  $\text{bcirc}(\mathcal{X})$  is defined as:

$$\text{bcirc}(\mathcal{X}) = \begin{bmatrix} X^{(1)} & X^{(n_3)} & \dots & X^{(2)} \\ X^{(2)} & X^{(1)} & \dots & X^{(3)} \\ \vdots & \vdots & \ddots & \vdots \\ X^{(n_3)} & X^{(n_3-1)} & \dots & X^{(1)} \end{bmatrix}$$

where,  $X^{(i)}$  represents the  $i$ -th frontal slice of tensor  $\mathcal{X}$ . Below is the definition of unfold.

$$\text{unfold}(\mathcal{Y}) = \begin{bmatrix} Y^{(1)} \\ Y^{(2)} \\ \vdots \\ Y^{(n_3)} \end{bmatrix}, \text{fold}(\text{unfold}(\mathcal{Y})) = \mathcal{Y}$$

The unfold operation in the above formula is a process that transforms a tensor into a matrix, resulting from unfolding the tensor into a matrix along a specific mode, enabling matrix-based operations. Unfold and fold are inverse operators of each other.

**Definition 2.** (Identity tensor [32]) For a tensor  $\mathcal{I} \in \mathbb{R}^{n_1 \times n_1 \times n_3}$ , if  $I^{(1)}$  is an identity matrix and  $I^{(i)}, i = 2, 3, 4 \dots n_3$  are zero matrices, then  $\mathcal{I}$  is called an identity tensor.

**Definition 3.** (f-diagonal tensor [32]) For a tensor  $\mathcal{S} \in \mathbb{R}^{n_1 \times n_1 \times n_3}$ , if all the frontal slices  $S^{(i)}, i = 2, 3, 4 \dots n_3$  in  $\mathcal{S}$  are diagonal matrices, then  $\mathcal{S}$  is called an f-diagonal tensor.

In fact, the decomposition process involves first applying a Fourier transform to the tensor, followed by providing the SVD decomposition of the matrix for each slice of the tensor.

**Definition 4.** (t-SVD tensor decomposition [14]) t-SVD decomposes a high-dimensional tensor into the product of lower-dimensional tensors. For a third-order tensor  $\mathcal{X} \in \mathbb{R}^{n_1 \times n_2 \times n_3}$ , if all the frontal slices  $S^{(i)}, i = 2, 3, 4 \dots n_3$  in  $\mathcal{S}$  are diagonal matrices, then the t-SVD decomposition can be expressed as:

$$\mathcal{X} = \mathcal{U} * \mathcal{S} * \mathcal{V}^*$$

where,  $\mathcal{S} \in \mathbb{R}^{n_1 \times n_2 \times n_3}$  is an f-diagonal tensor, and  $\mathcal{U} \in \mathbb{R}^{n_1 \times n_1 \times n_3}$  and  $\mathcal{V} \in \mathbb{R}^{n_2 \times n_2 \times n_3}$  are orthogonal tensors [26].

The rank corresponding to this decomposition is readily apparent.

**Definition 5.** (Tensor tubal rank [15]) For a given tensor  $\mathcal{X}_i \in \mathbb{R}^{d_I \times d_J \times K}$ , the tubal rank of the tensor, denoted as  $\text{rank}_t(\mathcal{X})$ , refers to the number of non-zero tubes in the t-SVD transformation.

$$\text{rank}_t(\mathcal{X}) = \#\{i : \mathcal{S}(i, i, :)\} = \max(r_1, r_2, \dots, r_{n_3})$$

**Definition 6.** (Tensor average rank [26]) For a third-order tensor  $\mathcal{X}_i \in \mathbb{R}^{n_1 \times n_2 \times n_3}$ , its nuclear norm derived from the t-product of tensors is defined as the sum of the singular values of the matrices obtained by unfolding the tensor along the third mode, expressed as:

$$\|\mathcal{X}\|_* = \frac{1}{n_3} \sum_{i=1}^{n_3} \|\bar{X}^{(i)}\|_*$$

where,  $\bar{X}^{(i)}$  is the  $i$ -th matrix obtained by unfolding  $\bar{\mathcal{X}}$  along the third mode.

When addressing the problem of minimizing tensor nuclear norm, it is essential to leverage the low-rank property of tensors. This is typically done by thresholding the singular values of tensors, ensuring the retention of lowrank properties and effective noise removal during the tensor completion process. We should adopt a suitable truncation method.

**Definition 7.** (Hard thresholding truncation of t-SVD decomposition, SVT) For a tubal singular value vector  $\bar{\sigma}_i^k$ , the hard thresholding truncation function is defined as follows:

$$\bar{f}_i^k(\bar{\sigma}_i^k, r) = \begin{cases} \bar{\sigma}_i^k, & \text{if } i \leq r \\ 0, & \text{otherwise} \end{cases}$$

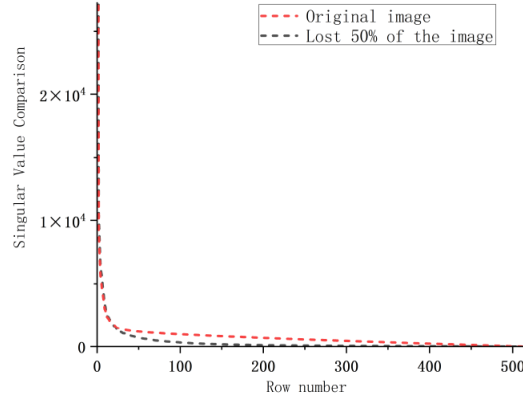
where,  $r$  is the singular value threshold, and the hard thresholding truncation function is a non-linear function that completely retains the larger singular values before the threshold while setting the singular values beyond the threshold to zero.

**Definition 8.** (The function of noise-based truncation methods) The noise estimate of the image is  $\mathcal{T}$ , and the function is as follows:

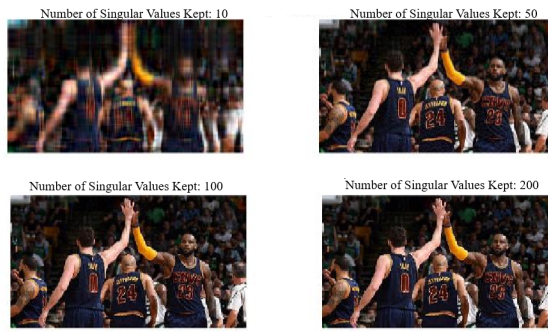
$$\bar{f}_i^k(\bar{\sigma}_i^k, \sigma_{\text{sample}}) = (\bar{\sigma}_i^k - \sigma_{\text{sample}})_+$$

where,  $\sigma_{\text{sample}} > 0$  is the noise estimate used as an adjustment parameter, and  $(\cdot)_+ = \max(\cdot, 0)$  is the soft thresholding function.

Subgraph (a) of Figure 1 compares the singular values of the original image and an image with a 50% missing rate. Subgraph (b) of Figure 1 shows images preserving the top 10, 50, 100, and 200 largest singular values, respectively.



(a)



(b)

**Figure 1.** (a) The singular values of the original image and an image with a 50% missing rate; (b) The images preserving the top 10, 50, 100, and 200 largest singular values, respectively

#### 4 Image Aggregation

In NLM denoising, we divide the image into sub-image blocks and search for similarity among these sub-blocks. After denoising using the mean, the subimage blocks are aggregated. Since the sub-image blocks overlap, the pixel points in the overlapping parts of the sub-data blocks are calculated using weighted summation. The weights are computed using Gaussian Euclidean distance, which considers the spatial distance within the local area, with the distance of the pixel to the center being proportional to its impact on the image. The formula for pixel fusion in the image is as follows:

$$\mathcal{X}(i, j, k) = \sum_{t \in \mathcal{Z}} \omega(i, j, k) t[\mathcal{X}_n(i, j, k)] \quad (2)$$

where, the indices  $(i, j, k)$  of  $\mathcal{X}_n(i, j, k)$  represent the position of each pixel point,  $\mathcal{Z}$  is the set covering the pixel point  $\mathcal{X}_{ijk}$ ,  $t[\mathcal{X}_n(i, j, k)]$  contains the gray value of the pixel point  $\mathcal{X}_n(i, j, k)$ , and  $\omega(i, j, k)$  is the Gaussian Euclidean distance weight of the data block.

The formula for calculating the Gaussian weight function  $\omega(i, j, k)$  is:

$$\omega(i, j, k) = \frac{1}{\sum_{t \in \mathcal{Z}} \exp\left(-\frac{DIS(\text{center } t[\mathcal{X}(i, j, k)], (i, j, k))^2}{2\sigma^2}\right)} \exp\left(-\frac{DIS(\text{center } t[\mathcal{X}(i, j, k)], (i, j, k))^2}{2\sigma^2}\right) \quad (3)$$

where,  $\text{center } t[\mathcal{X}(i, j, k)]$  represents the center of the data, and  $DIS(\text{center } t[\mathcal{X}(i, j, k)], (i, j, k))$  is the Euclidean distance from the center to the current pixel point.  $\sigma$  is the standard deviation of the Gaussian weight. The Gaussian weight function considers the relationship between distance and weight, resulting in a clearer and smoother aggregated image. The pixel fusion formula determines the pixels of the denoised image. The process includes image blocking, matching similar blocks, tensor completion denoising, and aggregation to obtain the final denoised image.

## 5 Proposed Model

$\mathcal{M}$  is a tensor image data corrupted by noise and missing pixels, with the objective to recover the data by combining NLM denoising [19] and tensor completion methods (TCTV) [29]. The basic idea of NLM denoising is to use the self-similarity of the image, averaging pixels with similar local structures to achieve denoising. For each pixel in the image, the NLM method calculates a weighted average based on the similarity between the pixel and other pixels in its neighborhood. The mathematical expression is:

$$\hat{I}(x) = \sum_{y \in \Omega} w(x, y) I(y)$$

where,  $\Omega$  is the set of observed pixels in the tensor, and  $w(x, y)$  is the weight determining the similarity between the pixels at positions  $x$  and  $y$ . The weight calculation formula is:

$$w(x, y) = \frac{1}{Z(x)} \exp\left(-\frac{\|I(N_x) - I(N_y)\|_2^2}{h^2}\right)$$

where,  $N_x$  and  $N_y$  are patches centered at pixel positions  $x$  and  $y$ , respectively.  $\|I(N_x) - I(N_y)\|_2^2$  is the  $L_2$  norm between the two patches.  $h$  is a filter parameter controlling the decay of the exponential function, and  $Z(x)$  is the normalization constant ensuring the sum of the weights is 1. The calculation formula for  $Z(x)$  is:

$$Z(x) = \sum_{y \in \Omega} \exp\left(-\frac{\|I(N_x) - I(N_y)\|_2^2}{h^2}\right)$$

The NLM method was originally proposed for grayscale images. For denoising color images, we can apply NLM to each channel of the image separately and then aggregate the denoised results of each channel to form a color image. Using NLM denoising promotes image smoothing, which works well in combination with completion methods that include TV regularization terms. Figure 2 shows a comparison of the completion effects of t-CTV combined with NLM, BM3D, and SVT combined with t-CTV. The PSNR and SSIM in the figure are the average values obtained from processing a set of data.

After applying NLM denoising utilizing the image's self-similarity, we obtain the tensor image  $\mathcal{X}$  to be completed. This low-rank tensor model can be formulated as a low-rank tensor completion problem (LRTC). The low-rank tensor completion problem can be represented by the following minimization model:

$$\min_{\mathcal{X}} \text{rank}(\mathcal{X}) \quad \text{s.t.} \quad \mathcal{P}_{\Omega}(\mathcal{X}) = \mathcal{P}_{\Omega}(\mathcal{Y}) \quad (4)$$

where,  $\mathcal{X}$  is the tensor to be solved,  $\mathcal{Y}$  is the observed tensor,  $\Omega$  is the set of indices of the observed elements, and  $\text{rank}()$  is the tensor rank function.

$$(\mathcal{P}_{\Omega}(\mathcal{X}))_{ijk} = \begin{cases} \mathcal{X}_{ijk}, & \text{if } (i, j, k) \in \Omega \\ 0, & \text{otherwise} \end{cases}$$

In the study of low-rank tensor completion (LRTC) problems, the rank function is usually used as a constraint to ensure that the completed tensor has a low rank. However, the rank function is non-convex, and directly minimizing the matrix rank is an NP-hard problem. To solve this problem, the nuclear norm is often used as the convex envelope of the rank function to approximate it, thus transforming the original non-convex optimization problem into a convex optimization problem.

$$\min_{\mathcal{X}} \|\mathcal{X}\|_* \quad \text{s.t.} \quad \mathcal{P}_{\Omega}(\mathcal{X}) = \mathcal{P}_{\Omega}(\mathcal{Y}) \quad (5)$$

The Total Variation (TV) regularization term helps preserve the edges and detail information of the image. It imposes a stronger penalty on smooth regions of the image, thereby reducing the information loss caused by smoothing, while imposing a smaller penalty on edge regions to preserve the details and structure of the image. Adding a TV regularization term to the above completion model:

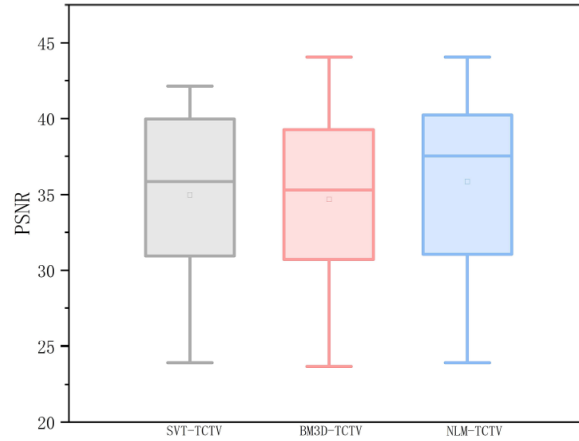
$$\min_{\mathcal{X}} \|\mathcal{X}\|_* + \lambda \|\mathcal{X}\|_{TV} \quad \text{s.t.} \quad \mathcal{P}_{\Omega}(\mathcal{X}) = \mathcal{P}_{\Omega}(\mathcal{Y}) \quad (6)$$

where,  $\lambda$  is a regularization parameter used to balance the TNN term and the TV regularization term for better performance.  $\|\mathcal{X}\|_{TV}$  is a regularization method used in image processing and computer vision to promote sparsity and edge preservation in images. The definition of  $\|\mathcal{X}\|_{TV}$  is:

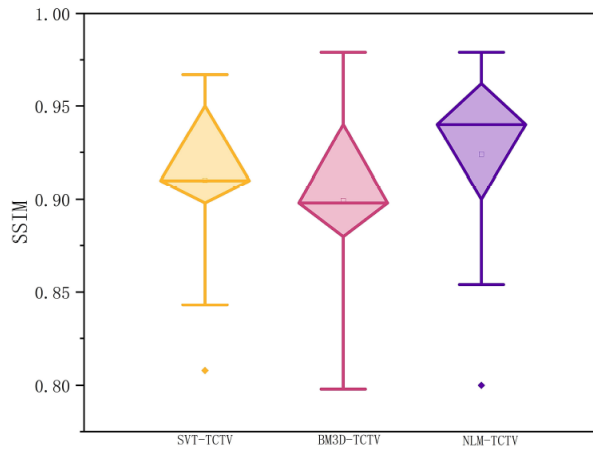
$$\|\mathcal{X}\|_{TV} = \|\nabla\mathcal{X}\|_1$$

For a tensor  $\mathcal{X} \in \mathbb{R}^{n_1 \times n_2 \times n_3 \dots n_k}$ , its gradient tensor unfolded along the third mode is represented as:

$$\nabla\mathcal{X}_{i_1 i_2 \dots i_k j} = \frac{\partial T_{i_1 i_2 \dots i_k}}{\partial x_j}$$



(a)



(b)

**Figure 2.** Comparison of different denoising methods

**Lemma 1.** Suppose  $\mathcal{T}_0 \in \mathbb{R}^{n_1 \times n_2 \times n_3 \dots \times n_d}$  has multiple prior structures, then the general tensor completion model can be expressed as:

$$\min_{\mathcal{T}} f(\mathcal{T}) = \sum \omega_i \|\mathcal{T}\|_{(i)} \quad \text{s.t.} \quad \mathcal{P}_{\Omega}(\mathcal{T}) = \mathcal{P}_{\Omega}(\mathcal{T}_0)$$

where,  $\|\cdot\|_{(i)}$  is a defined norm (such as TNN,  $L_2$ , Schatten -  $p$  norms, etc.), modeling a prior with Lipschitz constant  $L_i$ .  $\omega_i$  is weight parameter, and  $\Omega$  is the set of indices of the observed elements. If there exists a set of parameters or indices of observed positions such that  $\mathcal{T}_0$  is not the unique solution of the above equation, then the probability is at least  $1 - \exp\left(-\frac{c_1 m}{n_1 n_2 n_3 \dots n_d \|\widetilde{\mathcal{T}}_0\|_{\infty}^2}\right)$ , provided that

$$m \leq m_{\min} = \kappa_{\min}^2 n_1 n_2 n_3 \dots n_d$$

where,  $\kappa_{\min}^2 = \min \left\{ \kappa_i = \left\| \tilde{\mathcal{T}}_0 \right\|_1 / L_i \right\}$  and  $\tilde{\mathcal{T}}_0 = \mathcal{T}_0 / \|\mathcal{T}_0\|_F$ .

Lemma 1 [29] describes an interesting result [33] that in low-rank tensor completion, using two or more regularization terms is not necessarily better than using only one. In the study [29], the authors proposed the t-CTV model, which combines low-rank and smooth priors, and demonstrated that the unit ball of t-CTV has a significant similarity to the unit ball of the TV norm in its overall shape. Moreover, it shares some tight characteristics with TNN, such as the tangent planes of the two unit balls when viewed from the front, indicating a close relationship in constraining the solution space in terms of both low-rankness and smoothness.

**Definition 9.** (Tensor t-CTV Regularizer) For a given tensor  $\mathcal{X}_i \in \mathbb{R}^{n_1 \times n_2 \times n_3}$ , define  $\Gamma$  as the set of priors composed of directions L and S, and  $\nabla_3 \mathcal{X}$  as the gradient tensor unfolded along the third mode. The t-CTV regularizer is defined as:

$$\|\mathcal{X}\|_{\text{t-CTV}} = \sum_{k \in \Gamma} \frac{1}{\gamma} \|\nabla_k \mathcal{X}\|_{TNN}$$

where,  $\gamma$  is the cardinality of  $\Gamma$  used to balance the regularizer.

Based on the t-CTV regularizer, solving a tensor completion problem can be modeled as:

$$\min_{\mathcal{X}} \frac{1}{\gamma} \|\mathcal{X}\|_{\text{t-CTV}} \quad \text{subject to} \quad \mathcal{P}_{\Omega}(\mathcal{X}) = \mathcal{P}_{\Omega}(\mathcal{Y}) \quad (7)$$

We introduce auxiliary variables  $\mathcal{G}_k$ , and the problem is reformulated as:

$$\min_{\mathcal{X}, \mathcal{G}} \sum_{k \in \Gamma} \frac{1}{\gamma} \|\mathcal{G}_k\|_{*, \mathcal{L}} \quad \text{subject to} \quad \mathcal{P}_{\Omega}(\mathcal{X}) = \mathcal{P}_{\Omega}(\mathcal{Y}) \quad \mathcal{G}_k = \nabla_k \mathcal{X} \quad k \in \Gamma \quad (8)$$

With the preparations done, we solve the problem in equation (3.2) using the ADMM algorithm [34, 35]. The augmented Lagrangian function of equation (3.2) is defined as:

$$\begin{aligned} \mathcal{L}_{\rho}(\mathcal{X}, \mathcal{G}, \Lambda) = & \sum_{k \in \Gamma} \left( \frac{1}{\gamma} \|\mathcal{G}_k\|_{*, \mathcal{L}} + \langle \Lambda_k, \nabla_k \mathcal{X} - \mathcal{G}_k \rangle + \frac{\rho}{2} \|\nabla_k \mathcal{X} - \mathcal{G}_k\|_F^2 \right) + \iota_{\Omega}(\mathcal{X}) + \langle \Lambda, \mathcal{X} \rangle \\ & + \frac{\rho}{2} \|\mathcal{X} - \mathcal{M} + \mathcal{E}\|_F^2 + \frac{\beta}{2} \|\mathcal{X} - \mathcal{N}(\mathcal{X})\|_F^2 \end{aligned} \quad (9)$$

- $\Lambda_k$  is the Lagrange multiplier.
- $\rho$  is the penalty parameter.
- $\iota_{\Omega}(\mathcal{X})$  is the indicator function, defined as

$$\iota_{\Omega}(\mathcal{X}) = \begin{cases} 0 & \text{if } \mathcal{P}_{\Omega}(\mathcal{X}) = \mathcal{P}_{\Omega}(\mathcal{Y}) \\ +\infty & \text{otherwise} \end{cases}$$

Now, we solve the tensor completion problem (4.6) through the following steps:

- Initialize variables: Initialize  $\mathcal{X}$ ,  $\mathcal{G}_k$ , Lagrange multipliers  $\Lambda_k$ , and penalty parameter  $\rho$ .
- Update  $\mathcal{X}^{t+1}$ :

$$\mathcal{X}^{t+1} = \arg \min_{\mathcal{X}} \iota_{\Omega}(\mathcal{X}) + \sum_{k \in \Gamma} \left( \langle \Lambda_k^t, \nabla_k \mathcal{X} - \mathcal{G}_k^t \rangle + \frac{\rho}{2} \|\nabla_k \mathcal{X} - \mathcal{G}_k^t\|_F^2 \right) \quad (10)$$

The difference operations on tensors are proven to be linear through tensor-tensor products. We can apply multidimensional FFT to efficiently obtain the optimal solution for  $\mathcal{X}^{t+1}$  based on the convolution theorem of Fourier transforms:

$$\mathcal{X}_k^{t+1} = \mathcal{F}^{-1} \left( \frac{\mathcal{F}(\mathcal{P}_{\Omega}(\mathcal{X}_0)) - \mathcal{Y}^t + \mathcal{F}^t / \rho^t + \mathcal{H}}{1 + \sum_{k \in \Gamma} \mathcal{F}(\mathcal{D}_k)^T \circ \mathcal{F}(\mathcal{D}_k)} \right) \quad (11)$$

where,  $\mathcal{H} = \sum_{k \in \Gamma} \mathcal{F}(\mathcal{D}_k)^T \circ \mathcal{F}(\mathcal{G}_k^t - \frac{\Lambda_k^t}{\rho^t})$ , 1 is a tensor with all entries equal to 1,  $\circ$  denotes element-wise multiplication, and division is also element-wise.



- Update  $\mathcal{G}_k^{t+1}$ :

$$\mathcal{G}_k^{t+1} = \arg \min_{\mathcal{G}_k} \frac{1}{\gamma} \|\mathcal{G}_k\|_{*,\mathcal{L}} + \langle \Lambda_k^t, \nabla_k \mathcal{X}^{t+1} - \mathcal{G}_k \rangle + \frac{\rho}{2} \|\nabla_k \mathcal{X}^{t+1} - \mathcal{G}_k\|_F^2 \quad (12)$$

We solve this expression using Singular Value Thresholding (SVT), and the closed-form solution for this subproblem is given by:

$$\mathcal{G}_k^{t+1} = t - \text{SVT}_{1/\gamma\mu_t} (\nabla_k (\mathcal{X}^{t+1}) + \Lambda_k^t/\rho^k) \quad (13)$$

- Update Lagrange multipliers  $\Lambda_k^{t+1}$  and  $\gamma^{t+1}$ :

$$\Lambda_k^{t+1} = \Lambda_k^t + \rho (\nabla_k \mathcal{X}^{t+1} - \mathcal{G}_k^{t+1}), \quad k \in \Gamma \quad (14)$$

$$\gamma^{t+1} = \gamma^t + \rho (\mathcal{P}_\Omega(\mathcal{X}) - \mathcal{X}^{t+1} - \mathcal{Y}^{t+1}) \quad (15)$$

- Check convergence condition: Check the convergence condition. If the condition is met, terminate the iteration; otherwise, return to step 2.

$$\|\mathcal{L}^{t+1} - \mathcal{L}^t\| \leq \epsilon \quad (16)$$

Thus, based on the ADMM algorithm framework, we obtain the result:

$$\begin{cases} \mathcal{X}^{t+1} = \arg \min \mathcal{X} \iota_\Omega(\mathcal{X}) + \sum_{k \in \Gamma} \left( \langle \Lambda_k^t, \nabla_k \mathcal{X} - \mathcal{G}_k^t \rangle + \frac{\rho}{2} \|\nabla_k \mathcal{X} - \mathcal{G}_k^t\|_F^2 \right) \\ \mathcal{G}_k^{t+1} = \arg \min_{\mathcal{G}_k} \frac{1}{\gamma} \|\mathcal{G}_k\|_{*,\mathcal{L}} + \langle \Lambda_k^t, \nabla_k \mathcal{X}^{t+1} - \mathcal{G}_k \rangle + \frac{\rho}{2} \|\nabla_k \mathcal{X}^{t+1} - \mathcal{G}_k\|_F^2, \quad k \in \Gamma \\ \Lambda_k^{t+1} = \Lambda_k^t + \rho (\nabla_k \mathcal{X}^{t+1} - \mathcal{G}_k^{t+1}), \quad k \in \Gamma \\ \gamma^{t+1} = \gamma^t + \rho (\mathcal{P}_\Omega(\mathcal{X}) - \mathcal{X}^{t+1} - \mathcal{Y}^{t+1}) \end{cases} \quad (17)$$

## 6 Experimental Results

In this section, we conduct extensive experiments on computer vision images to demonstrate the superiority and effectiveness of the proposed method. For each LRTC method, we repeat the experiments five times on each type of data to avoid coincidences. All experiments are implemented on a Windows 10 platform with Matlab (R2016a), equipped with an Intel (R) Core (TM) i5-1035G1 1.00GHz CPU and 239GB of memory.

Evaluation Standards: This experiment uses Peak Signal-to-Noise Ratio (PSNR) and Structural Similarity Index (SSIM) to describe the quality of image recovery as evaluation metrics for color images (Table 1).

---

### Algorithm 1: ADMM for solving t-CTV-TC model

---

1. **Input:** Initialize  $\mathcal{X}$ ,  $\mathcal{G}_k$ , Lagrange multipliers  $\Lambda_k$ , and penalty parameter  $\rho$ .
2. **Update**  $\mathcal{X}^{t+1}$
3. **Update**  $\mathcal{G}_k^{t+1}$
4. **Update Lagrange multipliers**  $\Lambda_k^{t+1}$  and  $\gamma^{t+1}$
5. **Check convergence condition:**

$$\|\mathcal{L}^{t+1} - \mathcal{L}^t\| \leq \epsilon$$

If the condition is satisfied, terminate the iteration; otherwise, go back to step 2.

6. **End while**

7. **Output:**  $\mathcal{X} = \mathcal{X}^{t+1}$  and  $\hat{\epsilon} = \epsilon^{t+1}$
- 

### 6.1 Color Image Recovery

For the TC problem, we apply the proposed method to the task of repairing computer vision tensor data and compare it with five other tensor-based methods, namely HaLRTC [20], BCPF [36], KBR [37], and SNN-TV [38] and TNN-TV [39], which incorporate smooth priors. Commonly used computer vision images are employed, with each image size being  $512 \times 512 \times 3$ . Gaussian noise with a standard deviation of 0.01 is added to the experiments. Completing noisy color images is a significant and complex problem in computer vision, requiring algorithms to suppress noise while completing the images. Figure 3 shows the comparison with traditional methods on natural

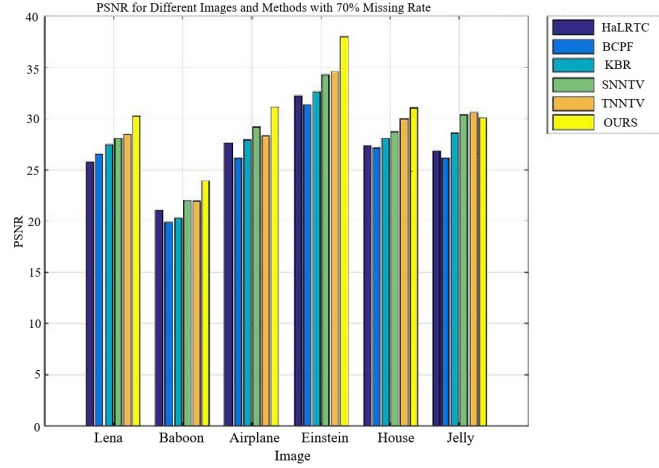
images under different missing rates (0.1, 0.3, 0.5, 0.7, 0.9). As seen from the results, our method achieves better recovery performance, particularly when the missing rate is high, and the image details are better preserved. The proposed method is more attentive to the features in the original image. From Figure 4, comparing PSNR and SSIM of various methods, it is clear that the obtained images generally have higher PSNR and lower, SSIM values than other methods. After denoising with NLM, the image is smoother, and the completed edges are clearer. The recovery results indicate that this method can effectively restore the image.

**Table 1.** PSNR and SSIM for different images and completion methods

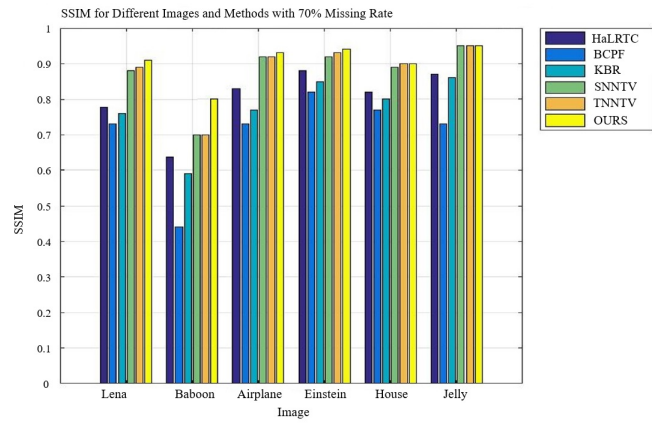
Image	Missing Rate	HaLRTC		BCPF		KBR		SNNTV		TNNTV		OURS	
		PSNR	SSIM	PSNR	SSIM	PSNR	SSIM	PSNR	SSIM	PSNR	SSIM	PSNR	SSIM
Lena	0.1	37.66	0.97	33.61	0.93	39.13	0.97	37.82	0.98	38.23	0.98	40.24	0.98
	0.3	33.54	0.95	32.38	0.91	35.73	0.98	34.32	0.96	34.85	0.97	37.95	0.97
	0.5	29.82	0.90	29.87	0.85	31.67	0.89	31.32	0.97	31.74	0.94	34.68	0.95
	0.7	25.77	0.78	26.56	0.73	27.42	0.76	28.04	0.88	28.45	0.89	30.23	0.91
	0.9	19.74	0.46	20.29	0.40	18.56	0.31	22.59	0.69	23.58	0.72	20.23	0.52
Baboon	0.1	32.60	0.98	21.78	0.95	34.32	0.98	32.51	0.98	32.65	0.98	34.10	0.97
	0.3	27.28	0.92	20.69	0.54	28.23	0.92	27.42	0.93	27.40	0.93	29.68	0.95
	0.5	23.92	0.82	20.50	0.50	24.15	0.80	24.41	0.85	24.28	0.85	26.67	0.90
	0.7	21.08	0.64	19.87	0.44	20.28	0.59	21.98	0.70	21.87	0.70	23.92	0.80
	0.9	17.99	0.34	17.87	0.40	15.97	0.28	19.21	0.41	19.54	0.42	18.24	0.48
Airplane	0.1	38.72	0.97	28.08	0.81	39.35	0.97	38.94	0.97	38.68	0.97	40.53	0.97
	0.3	35.63	0.96	27.80	0.78	36.03	0.95	36.42	0.97	34.59	0.97	38.45	0.97
	0.5	32.06	0.92	27.48	0.74	32.76	0.90	33.29	0.95	31.44	0.95	35.26	0.96
	0.7	27.57	0.83	26.17	0.73	27.88	0.77	29.16	0.92	28.33	0.92	31.17	0.93
	0.9	21.39	0.57	21.93	0.50	19.60	0.44	23.44	0.78	23.83	0.79	24.85	0.81
Einstein	0.1	39.53	0.97	32.83	0.86	40.05	0.99	39.64	0.97	39.78	0.97	41.73	0.97
	0.3	38.00	0.96	32.81	0.86	38.87	0.95	38.48	0.96	38.77	0.97	41.29	0.98
	0.5	35.64	0.94	32.50	0.82	36.68	0.93	36.75	0.94	37.06	0.95	40.23	0.95
	0.7	32.22	0.88	31.39	0.82	32.67	0.85	34.26	0.92	34.61	0.93	37.93	0.94
	0.9	26.14	0.72	27.86	0.68	21.45	0.49	29.03	0.83	29.85	0.84	30.34	0.86
House	0.1	38.28	0.97	31.21	0.93	38.90	0.97	38.61	0.97	38.77	0.97	38.94	0.96
	0.3	35.03	0.95	31.17	0.88	35.78	0.95	35.82	0.96	35.79	0.96	37.52	0.95
	0.5	31.65	0.92	29.79	0.85	31.97	0.89	32.92	0.94	32.91	0.94	35.32	0.94
	0.7	27.34	0.82	27.16	0.77	28.09	0.80	28.70	0.89	29.89	0.90	31.06	0.90
	0.9	21.10	0.57	21.46	0.49	20.26	0.38	23.08	0.76	24.29	0.78	22.32	0.58
Jelly	0.1	38.92	0.97	31.60	0.95	39.38	0.97	39.24	0.97	39.28	0.97	43.42	0.99
	0.3	35.74	0.96	31.04	0.93	36.75	0.96	37.03	0.97	37.08	0.97	40.01	0.98
	0.5	31.73	0.94	29.54	0.91	33.44	0.93	34.22	0.97	34.30	0.97	36.18	0.98
	0.7	26.85	0.87	26.19	0.73	28.62	0.86	30.33	0.95	30.62	0.95	30.10	0.95
	0.9	20.16	0.64	19.74	0.58	19.16	0.54	23.13	0.82	24.26	0.85	21.51	0.72



**Figure 3.** Visual comparison of color images completed using different methods



(a)



(b)

**Figure 4.** PSNR and SSIM comparison under a loss rate of 70%

## 6.2 Medical Image Recovery

We evaluate the performance of our method on some computed tomography (CT) images and brain nuclear magnetic resonance imaging (MRI) images. Both are commonly used tensor data.

CT and MRI images are commonly used medical imaging modalities that provide comprehensive diagnostic information for medical diagnoses. Figure 5 shows the image recovery results and corresponding PSNR and SSIM values obtained under sampling rates of 0.2 and 0.3, with a noise standard deviation level of 0.02. Through direct observation, we found that the images obtained using the TNN-TV, t-CTV, and t-CTV-NLM methods were clearer compared to other methods. These tensor nuclear norm truncation-based methods preserved more image details, resulting in high-resolution images with sharp, non-blurry edges, which are beneficial for further diagnosis. The visual results of the medical images clearly demonstrate the excellent performance of these methods in restoring medical image data. Using the evaluation data, the PSNR of these methods is the highest, with an improvement of 2-3dB, and the SSIM value increases by 0.06 to 0.12. Moreover, under severe noise interference, the NLM denoiser effectively removes more noise and smooths the images, making the effect of NLM-TCTV particularly significant. This further proves the effectiveness and robustness of the method in restoring medical images in high-noise environments.

## 6.3 Remote Sensing Image Recovery

Satellite water images, based on satellite remote sensing technology, are specifically used to monitor and analyze the state of water bodies. The multispectral and hyperspectral images in satellite water maps contain dozens or even hundreds of spectral bands, forming a high-dimensional tensor. Figure 6 shows the effects of different completion methods on panchromatic satellite water maps. The sampling rates of the images are 0.5, 0.2, 0.4, 0.4, and 0.5, respectively. By intuitively observing the images processed by various methods, we find that the images processed by the SNN method exhibit some blurring of features. After adding the TV regularization term, the images become

smoother, and the features are more prominent. Our method generally maintains a significant quantitative advantage, with PSNR and SSIM values of most images being optimal in the NLM-TCTV method. Compared to the suboptimal methods, the PSNR of our method is improved by 0.5-1dB. However, when the sampling rate is low, due to more missing blocks, the effect of block matching based on image self-similarity is not significant. In this case, NLM-TCTV is not the optimal method, but it shows only a slight difference compared to the t-CTV method without the NLM denoiser. Overall, our method enables more structural information to be observed in missing images, and the obtained results are closer to the original, showing excellent performance in the field of satellite remote sensing water maps.

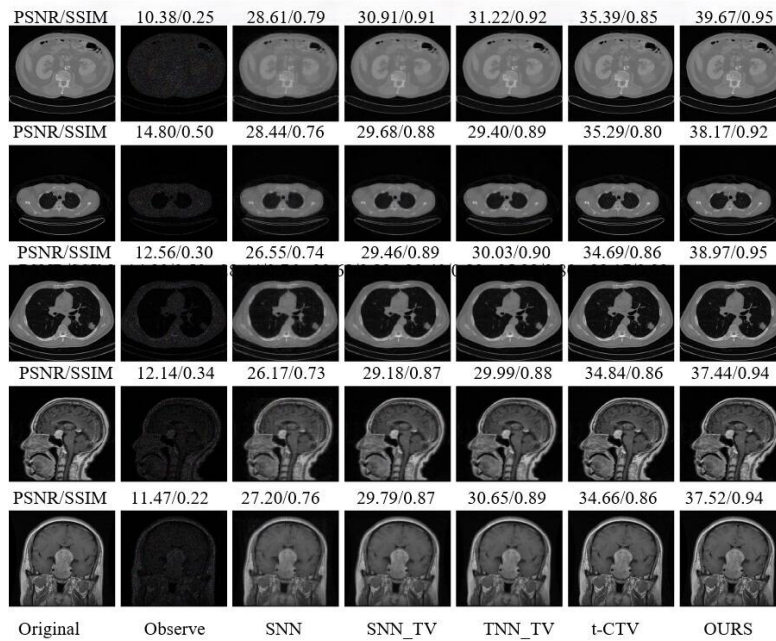


**Figure 5.** Completion of medical images using different completion methods

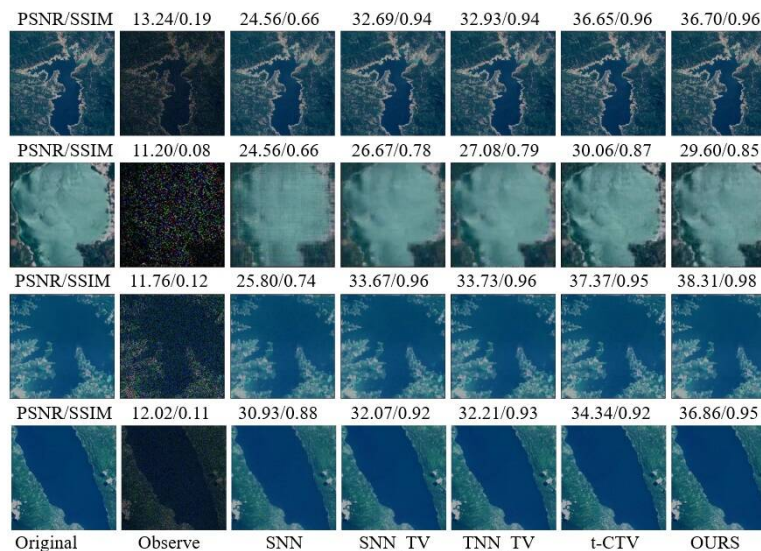


**Figure 6.** Different completion methods for satellite water image inpainting

## 7 Conclusions

In this study, inspired by the invertible linear transform-based t-product, which generalizes the existing t-product based on discrete Fourier transform, we provided a more general definition of the tubal rank and tensor nuclear norm. We explored the t-CTV norm, which incorporates both low-rank and smooth priors simultaneously. This regularization term improves the completion effect by combining both low-rank and smooth priors. When facing

tensor completion problems with noise, many methods cannot accurately distinguish between noise and the missing pixels, affecting the completion results. The incorporation of methods utilizing the non-local similarity of images, such as NLM, not only enhances image quality but also strengthens image smoothness, achieving excellent results. Through experiments and theoretical proof, it is shown that the NLM-TCTV model is convergent and feasible.

We will attempt to validate more tensor recovery tasks, such as outlier detection and background extraction, by incorporating this regularizer into the corresponding models to further verify its effectiveness. Although the t-CTV model proposed in this paper has achieved significant results in the tensor completion problem, there are still some directions worth further research and improvement. The current ADMM algorithm, though effective, has high computational complexity for large-scale tensor data. Future work can consider enhancing computational efficiency through parallel computing and optimization algorithms. The selection of hyperparameters such as the penalty parameter  $\rho$  and step size  $\gamma$  significantly affects the algorithm's performance. Future work could consider using adaptive parameter selection methods or learning algorithms to automatically adjust the parameters. In summary, the NLM-TCTV model provides an effective solution to the tensor completion problem and proposes a new d-order tensor recovery model. Future research can further explore and improve in aspects such as algorithm optimization, parameter selection, application extension, and theoretical analysis. Next, we will combine additional prior knowledge, image enhancement techniques, and optimization methods based on low-rankness to enhance its performance and applicability in practical applications.

### Data Availability

The data used to support the research findings are available from the corresponding author upon request.

### Conflicts of Interest

The authors declare no conflict of interest.

### References

- [1] W. Liu, M. Haardt, M. S. Greco, C. F. Mecklenbräuker, and P. Willett, "Twenty-five years of sensor array and multichannel signal processing: A review of progress to date and potential research directions," *IEEE Signal Process. Mag.*, vol. 40, no. 4, pp. 80–91, 2023. <https://doi.org/10.1109/MSP.2023.3258060>
- [2] M. H. Wang, D. F. Hong, Z. Han, J. X. Li, J. Yao, L. R. Gao, B. Zhang, and J. Chanussot, "Tensor decompositions for hyperspectral data processing in remote sensing: A comprehensive review," *IEEE Geosci. Remote Sens. Mag.*, vol. 11, no. 1, pp. 26–72, 2023. <https://doi.org/10.1109/MGRS.2022.3227063>
- [3] H. Y. Li, S. Knapik, Y. F. Li, C. Park, J. C. Guo, S. Mojumder, Y. Lu, W. Chen, D. W. Apley, and W. K. Liu, "Convolution Hierarchical Deep-Learning Neural Network Tensor Decomposition (C-HiDeNN-TD) for high-resolution topology optimization," *Comput. Mech.*, vol. 72, pp. 363–382, 2023. <https://doi.org/10.1007/s00466-023-02333-8>
- [4] J. Liu, S. J. Li, J. Zhang, and P. Zhang, "Tensor networks for unsupervised machine learning," *Phys. Rev. E*, vol. 107, no. L012103, 2023. <https://doi.org/10.1103/PhysRevE.107.L012103>
- [5] L. L. Feng, C. Zhu, Z. Long, J. N. Liu, and Y. P. Liu, "Multiplex transformed tensor decomposition for multidimensional image recovery," *IEEE Trans. Image Process.*, vol. 32, pp. 3397–3412, 2023. <https://doi.org/10.1109/TIP.2023.3284673>
- [6] S. J. Xia, D. Qiu, and X. J. Zhang, "Tensor factorization via transformed tensor-tensor product for image alignment," *Numer. Algor.*, vol. 95, no. 3, pp. 1251–1289, 2024. <https://doi.org/10.1007/s11075-023-01607-9>
- [7] Y. Xu, Z. B. Wu, J. Chanussot, and Z. H. Wei, "Nonlocal patch tensor sparse representation for hyperspectral image super-resolution," *IEEE Trans. Image Process.*, vol. 28, no. 6, pp. 3034–3047, 2019. <https://doi.org/10.1109/TIP.2019.2893530>
- [8] D. L. Donoho, "Compressed sensing," *IEEE Trans. Inf. Theory*, vol. 52, no. 4, pp. 1289–1306, 2006. <https://doi.org/10.1109/TIT.2006.871582>
- [9] E. J. Candes and T. Tao, "Decoding by linear programming," *IEEE Trans. Inf. Theory*, vol. 51, no. 12, pp. 4203–4215, 2005. <https://doi.org/10.1109/TIT.2005.858979>
- [10] H. A. L. Kiers, "Towards a standardized notation and terminology in multiway analysis," *J. Chemometrics*, vol. 14, no. 3, pp. 105–122, 2000. [https://doi.org/10.1002/1099-128X\(200005/06\)14:3<105::AID-CEM582>3.0.CO;2-I](https://doi.org/10.1002/1099-128X(200005/06)14:3<105::AID-CEM582>3.0.CO;2-I)
- [11] C. J. Hillar and L. H. Lim, "Most tensor problems are NP-hard," *J. ACM*, vol. 60, no. 6, pp. 1–39, 2013. <https://doi.org/10.1145/2512329>
- [12] L. R. Tucker, "Some mathematical notes on three-mode factor analysis," *Psychometrika*, vol. 31, no. 3, pp. 279–311, 1966. <https://doi.org/10.1007/BF02289464>
- [13] T. G. Kolda and B. W. Bader, "Tensor decompositions and applications," *SIAM Rev.*, vol. 51, no. 3, pp. 455–500, 2009. <https://doi.org/10.1137/07070111X>

- [14] M. E. Kilmer and C. D. Martin, "Factorization strategies for third-order tensors," *Linear Algebra Appl.*, vol. 435, no. 3, pp. 641–658, 2011. <https://doi.org/10.1016/j.laa.2010.09.020>
- [15] Z. M. Zhang, G. Ely, S. C. Aeron, N. Hao, and M. Kilmer, "Novel methods for multilinear data completion and de-noising based on tensor-SVD," in *Proceedings of the IEEE Conference on Computer Vision and Pattern Recognition (CVPR)*, Columbus, OH, USA, 2014, pp. 3842–3849. <https://doi.org/10.1109/CVPR.2014.485>
- [16] X. J. Zhang and M. K. Ng, "Low rank tensor completion with Poisson observations," *IEEE Trans. Pattern Anal. Mach. Intell.*, vol. 44, no. 8, pp. 4239–4251, 2021. <https://doi.org/10.1109/TPAMI.2021.3059299>
- [17] A. D. Wang, Z. Jin, and G. Q. Tang, "Robust tensor decomposition via t-SVD: Near-optimal statistical guarantee and scalable algorithms," *Signal Process.*, vol. 167, p. 107319, 2020. <https://doi.org/10.1016/j.sigpro.2019.107319>
- [18] T. Li and J. W. Ma, "T-SVD based non-convex tensor completion and robust principal component analysis," in *2020 25th International Conference on Pattern Recognition (ICPR)*, Milan, Italy, 2021, pp. 6980–6987. <https://doi.org/10.1109/ICPR48806.2021.9412248>
- [19] A. Buades, B. Coll, and J. M. Morel, "A non-local algorithm for image denoising," in *2005 IEEE Computer Society Conference on Computer Vision and Pattern Recognition (CVPR'05)*, San Diego, CA, USA, 2005, pp. 60–65. <https://doi.org/10.1109/CVPR.2005.38>
- [20] J. Liu, P. Musialski, P. Wonka, and J. P. Ye, "Tensor completion for estimating missing values in visual data," *IEEE Trans. Pattern Anal. Mach. Intell.*, vol. 35, no. 1, pp. 208–220, 2012. <https://doi.org/10.1109/TPAMI.2012.39>
- [21] D. Goldfarb and Z. W. Qin, "Robust low-rank tensor recovery: Models and algorithms," *SIAM J. Matrix Anal. Appl.*, vol. 35, no. 1, pp. 225–253, 2014. <https://doi.org/10.1137/130905010>
- [22] J. A. Bengua, H. N. Phien, H. D. Tuan, and M. N. Do, "Efficient tensor completion for color image and video recovery: Low-rank tensor train," *IEEE Trans. Image Process.*, vol. 26, no. 5, pp. 2466–2479, 2017. <https://doi.org/10.1109/TIP.2017.2672439>
- [23] X. J. Zhang, "A nonconvex relaxation approach to low-rank tensor completion," *IEEE Trans. Neural Netw. Learn. Syst.*, vol. 30, no. 6, pp. 1659–1671, 2019. <https://doi.org/10.1109/TNNLS.2018.2872583>
- [24] O. Semerci, N. Hao, M. E. Kilmer, and E. L. Miller, "Tensor-based formulation and nuclear norm regularization for multienergy computed tomography," *IEEE Trans. Image Process.*, vol. 23, no. 4, pp. 1678–1693, 2014. <https://doi.org/10.1109/TIP.2014.2305840>
- [25] Z. M. Zhang and S. Aeron, "Exact tensor completion using t-SVD," *IEEE Trans. Signal Process.*, vol. 65, no. 6, pp. 1511–1526, 2016. <https://doi.org/10.1109/TSP.2016.2639466>
- [26] C. Y. Lu, J. S. Feng, Y. D. Chen, W. Liu, Z. C. Lin, and S. C. Yan, "Tensor robust principal component analysis with a new tensor nuclear norm," *IEEE Trans. Pattern Anal. Mach. Intell.*, vol. 42, no. 4, pp. 925–938, 2020. <https://doi.org/10.1109/TPAMI.2019.2891760>
- [27] C. Y. Lu, X. Peng, and Y. C. Wei, "Low-rank tensor completion with a new tensor nuclear norm induced by invertible linear transforms," in *2019 IEEE/CVF Conference on Computer Vision and Pattern Recognition (CVPR)*, Long Beach, CA, USA, 2019, pp. 5989–5997. <https://doi.org/10.1109/CVPR.2019.00615>
- [28] C. J. Pan, C. Ling, H. J. He, L. Qi, and Y. W. Xu, "Sparse+ Low-Rank tensor completion approach for recovering images and videos," *Signal Process. Image Commun.*, vol. 127, p. 117152, 2024. <https://doi.org/10.1016/j.image.2024.117152>
- [29] H. L. Wang, J. J. Peng, W. J. Qin, J. J. Wang, and D. Y. Meng, "Guaranteed tensor recovery fused low-rankness and smoothness," *IEEE Trans. Pattern Anal. Mach. Intell.*, vol. 45, no. 9, pp. 10990–11007, 2023. <https://doi.org/10.1109/TPAMI.2023.3259640>
- [30] L. Xu, L. Cheng, N. Wong, and Y. C. Wu, "Tensor train factorization under noisy and incomplete data with automatic rank estimation," *Pattern Recognit.*, vol. 141, p. 109650, 2023. <https://doi.org/10.1016/j.patcog.2023.109650>
- [31] P. L. Wu, X. L. Zhao, M. Ding, Y. B. Zheng, L. B. Cui, and T. Z. Huang, "Tensor ring decomposition-based model with interpretable gradient factors regularization for tensor completion," *Knowl. Based Syst.*, vol. 259, p. 110094, 2023. <https://doi.org/10.1016/j.knosys.2022.110094>
- [32] W. J. Qin, H. L. Wang, F. Zhang, J. J. Wang, X. Luo, and T. W. Huang, "Low-rank high-order tensor completion with applications in visual data," *IEEE Trans. Image Process.*, vol. 31, pp. 2433–2448, 2022. <https://doi.org/10.1109/TIP.2022.3155949>
- [33] S. Oymak, A. Jalali, M. Fazel, Y. C. Eldar, and B. Hassibi, "Simultaneously structured models with application to sparse and low-rank matrices," *IEEE Trans. Inf. Theory*, vol. 61, no. 5, pp. 2886–2908, 2015. <https://doi.org/10.1109/TIT.2015.2401574>
- [34] S. Boyd, N. Parikh, E. Chu, B. Peleato, and J. Eckstein, "Distributed optimization and statistical learning via the alternating direction method of multipliers," *Found. Trends Mach. Learn.*, vol. 3, no. 1, pp. 1–122, 2011. <http://doi.org/10.1561/22000000016>

- [35] C. Y. Lu, J. S. Feng, S. C. Yan, and Z. C. Lin, “A unified alternating direction method of multipliers by majorization minimization,” *IEEE Trans. Pattern Anal. Mach. Intell.*, vol. 40, no. 3, pp. 527–541, 2018. <https://doi.org/10.1109/TPAMI.2017.2689021>
- [36] Q. B. Zhao, L. Q. Zhang, and A. Cichocki, “Bayesian CP factorization of incomplete tensors with automatic rank determination,” *IEEE Trans. Pattern Anal. Mach. Intell.*, vol. 37, no. 9, pp. 1751–1763, 2015. <https://doi.org/10.1109/TPAMI.2015.2392756>
- [37] Q. Xie, Q. Zhao, D. Y. Meng, and Z. B. Xu, “Kronecker-basis-representation based tensor sparsity and its applications to tensor recovery,” *IEEE Trans. Pattern Anal. Mach. Intell.*, vol. 40, no. 8, pp. 1888–1902, 2018. <https://doi.org/10.1109/TPAMI.2017.2734888>
- [38] X. T. Li, Y. M. Ye, and X. F. Xu, “Low-rank tensor completion with total variation for visual data inpainting,” in *Proceedings of the AAAI Conference on Artificial Intelligence*, San Francisco, California, USA, 2017. <https://doi.org/10.1609/aaai.v31i1.10776>
- [39] D. Qiu, M. R. Bai, M. K. Ng, and X. J. Zhang, “Robust low-rank tensor completion via transformed tensor nuclear norm with total variation regularization,” *Neurocomputing*, vol. 435, pp. 197–215, 2021. <https://doi.org/10.1016/j.neucom.2020.12.110>